

C₁N₁ Thin Films from Guanine Decomposition Fragments

Mária Jerigová, Julian Heske, Thomas D. Kühne, Zhihong Tian, Michael Tovar, Mateusz Odziomek, and Nieves López-Salas*

Polymeric semiconductors are finding a wide range of applications. In particular, graphitic carbon nitride g-C₃N₄ has been investigated extensively in the past decade. However, the family of carbon nitrides is not limited to C₃N₄ and new C_xN_y are now being explored due to their different bandgap energy, morphology, and overall physicochemical properties. Here, homogenous and semi-transparent C₁N₁ thin films are fabricated using guanine as a nontoxic molecular precursor. They are synthesized in a simplified chemical vapor deposition process on top of fused silica and fluorine doped tin oxide coated glass substrates. The chemical and structural studies reveal that C/N ratio is close to target 1, triazine vibrations are visible in vibrational spectra and stacking of the film is observed from glancing incidence X-ray diffraction data. The (photo)electrochemical properties are studied, the film is a p-type semiconductor with a good photoresponse to visible light and a suitable catalyst for hydrogen evolution reaction. A simple and safe way of synthesizing C₁N₁ films on a range of substrates is presented here.


2015, many studies have been published on C₂N.^[3] The bandgap of C₂N is 1.96 eV, narrower than the one of g-C₃N₄ (2.7 eV), thus offering better visible light absorption. C₂N is promising in catalytic, electrocatalytic, and photocatalytic applications.^[4] Theoretical studies show that the value of valence and conduction band can be tuned and the water redox potentials lie between the valence and conduction bands, which makes it a potential candidate for water splitting.^[5] Theoretical studies performed decades ago also postulated the existence of 2D structures of C₃N materials.^[6] However, it was not until 2016 when Baek et al. successfully synthesized C₃N nanocrystals for the first time.^[7] Its experimental bandgap was 2.67 eV, thus broader than that of C₂N, indicating limited photocatalytic applicability compared to C₂N.^[7]

Another member of the carbon nitride family is C₁N₁. Likewise, it was a subject of many theoretical studies, which predicted the C₁N₁ structure to be a semiconductor with a direct bandgap in the range of 2.89–2.72 eV, which is a bit broader than that of g-C₃N₄.^[8] The main interest is to use the material in applications like electro(photo)catalysis and hydrogen storage.^[4] However, C₁N₁ materials attracted much less attention, perhaps due to the problems of synthesizing them. Up to date, the reports on the synthesis of C₁N₁ materials are very limited. Most use tricyanotriazine^[9] or trichlorotriazine^[10] as a starting compound. These compounds are both harsh and toxic chemicals. Furthermore, the structural analysis of the resulting materials points to the presence of very distorted structures with elements not corresponding to model C₁N₁. Ordered materials were obtained only by the incorporation of

1. Introduction

Polymeric semiconductors find a wide range of applications in energy, electronics, or photo(electro)catalysis.^[1] In particular, the graphitic carbon nitride, g-C₃N₄, has gained enormous attention because of its relatively narrow bandgap, chemical inertness, and chemical composition made of abundant elements.^[2] However, the family of carbon nitrides is not limited to C₃N₄. Many theoretical studies have shown that modulating the C/N ratio tunes properties like the bandgap energy or the energy of valence and conduction bands. The electronic properties of C_xN_y phases can further be modulated by controlling the thickness, elemental doping, and construction of heterojunctions. After Baek et al. synthesized and characterized C₂N crystal in

M. Jerigová, M. Odziomek, N. López-Salas
Colloid Chemistry Department
Max Planck Institute of Colloids and Interfaces
Am Mühlenberg 1, 14476 Potsdam, Germany
E-mail: ieves.lopezsalas@mpikg.mpg.de

 The ORCID identification number(s) for the author(s) of this article can be found under <https://doi.org/10.1002/admi.202202061>.

© 2022 The Authors. Advanced Materials Interfaces published by Wiley-VCH GmbH. This is an open access article under the terms of the Creative Commons Attribution License, which permits use, distribution and reproduction in any medium, provided the original work is properly cited.

DOI: 10.1002/admi.202202061

J. Heske, T. D. Kühne
Dynamics of Condensed Matter and Center
for Sustainable Systems Design
Chair of Theoretical Chemistry
University of Paderborn
Warburger Str. 100, D-33098 Paderborn, Germany

Z. Tian
Engineering Research Center for Nanomaterials
Henan University
Kaifeng 475004, P. R. China

M. Tovar
Department Structure and Dynamics of Energy Materials
Helmholtz-Zentrum Berlin für Materialien und Energie
Hahn-Meitner-Platz 1, 14109 Berlin, Germany

metals into the structure. Feng et al.^[10c] used copper foil, which directs the layer by layer growth and coordinates inside the cavity of the C_1N_1 structure as CuCl. After removing the copper by acid washing, the structure collapses and becomes amorphous. All previous research reports describe the formation of amorphous bulk powders which strongly limits their potential applications and shows the necessity to develop new reliable synthetic approaches yielding crystalline structures either in the form of bulk powder or homogenous films.

Here, we present the direct synthesis of C_1N_1 thin films through a simplified chemical vapor deposition (CVD) process using guanine as a precursor. Guanine, like all nucleobases, is essentially an oligomer of HCN,^[11] which makes it a potential source of nitrogen-rich carbonaceous compounds upon thermal decomposition and condensation. It has been shown, that guanine releases cyano-containing species upon collision-induced dissociation in the gas phase.^[12] Here, we confirm the presence of cyano-species in thermal decomposition products of guanine, which can further condense on a substrate surface, creating C_1N_1 films. The one-step thermal CVD process offers ease of large-scale production and consequent application. The thermal energy is used to decompose guanine, and the decomposition products then react on top of a substrate. In such a setup, toxic cyano compounds are only present as intermediates in the reaction, therefore offering an advantage to previous reports of C_1N_1 materials. Physical characteristics of prepared samples are studied together with the (photo)electrochemical behavior, showing a range of potential applications.

2. Results and Discussion

The thin films were prepared by condensation of thermal decomposition products of guanine on top of fused silica substrate in a simplified thermal CVD process. The schematic of the setup is shown in **Figure 1a**. The guanine was placed at the end of a test tube with fused silica substrate at the other end. The test tube was then placed in a chamber oven with a nitrogen flow and heated up to 500 °C for 1 h. The process creates a homogeneous brown film on the top of a substrate (see **Figure 1b**). To elucidate the mechanism of the process the thermogravimetric analysis (TGA) of guanine coupled with analysis of gaseous products by mass spectroscopy (MS) and Fourier-transform infrared spectroscopy (FTIR) was performed (**Figure 1c,d**). Guanine starts decomposing at temperatures above 400 °C which is indicated by a sharp mass loss of about 60% up to 500 °C. The mass loss continues with a lower rate up to a plateau at 800 °C, as shown in **Figure 1c**. Unlike other nucleobases, guanine does not sublimate due to stronger molecular hydrogen bonding, instead it decomposes.^[13] The intensive evolution of gaseous products starts at about 450 °C. First detected products are ammonia (m/z 17 and FTIR peaks at 928, 965, and 3337 cm^{-1}), cyanic or isocyanic acid (m/z 43 and FTIR peaks at 2250 and 2280 cm^{-1}) and HCN (m/z 27 and FTIR peak at 716 cm^{-1}). Those are rather typical species released upon decomposition of HCN-based oligomers.^[14] CO_2 (m/z 44 and FTIR peak at 2365 cm^{-1}) was also detected using both techniques. However, the large drop of the m/z 32 ion current observed with the concomitant appearance of m/z 44 ion

current indicates that CO_2 is the product of the reaction of guanine with residual oxygen in the system.

The results indicate that the film is formed through the deposition of guanine decomposition products which undergo a thermal condensation process. This allows the fabrication of CN films avoiding direct use of toxic cyano-compounds as reagents. Moreover, the cyano-compounds are released and interact at higher temperatures than using other volatile precursors, such as dicyanamide. There are numerous pathways of condensation of HCN, HCNO/HNCO, and NH_3 . However, these pathways are difficult to predict at such high temperatures, especially that they might induce formation of radical species. We hypothesize that the formation of the films starts with the well-known rapid trimerization of isocyanic acid to cyanuric acid and the generation of a triazine derivative which is a building block for many C_xN_y phases including C_1N_1 . The missing C–C bond could potentially be formed by nucleophilic addition of HCN to the carbonyl group from triene tautomer of cyanuric acid. The dehydration of the formed hydroxynitril would form a nitril derivative of cyanuric acid which ideal condensation would directly produce the model C_1N_1 phase.

Based on TGA analysis, 500 °C was chosen as the optimal temperature for a release of film-forming molecules. The CVD-like process allows the molecular precursors to arrange in an ordered way on top of a substrate. Scanning electron microscopy (SEM) revealed the homogeneous and smooth morphology of the film on a microscopic level (**Figure S1a**, Supporting Information). Atomic force microscopy (AFM) analysis of the film also shows a smooth surface with minimal roughness of 3 nm (**Figure S1b**, Supporting Information). The thickness of the film as determined by AFM is 78 nm. The chemical composition of the film measured by energy dispersive X-ray analysis (EDX) revealed an atomic C/N ratio of 0.93, which is close to the targeted C_1N_1 phase. The composition was also confirmed by elemental chemical analysis of the sample prepared on top of a glass substrate. Unlike samples prepared on top of fused silica, the sample on top of glass can be peeled by simple immersion in water. The C/N ratio obtained was 1.2. Here it is important to notice that the samples might adsorb CO_2 and H_2O , which could lead to changes in the C/N ratio as the analysis is not carried out under vacuum. Structural features and bonding in the film were studied using FTIR (**Figure 2a**). The broad band around 3200 cm^{-1} relates to the presence of –OH groups most likely from adsorbed water, and an additional peak at 3300 comes from –NH groups indicating the incomplete condensation of guanine decomposition products. The broad band between 1600 and 1200 cm^{-1} is typical for conjugated C–N structures. Moreover, the bands at 1365 and 1582 cm^{-1} suggest the presence of C=C and C=N.^[9b] The presence of triazine is supported by a peak at 766 cm^{-1} which can be seen when using an fluorine doped tin oxide (FTO) coated glass substrate (**Figure S3**, Supporting Information). Therefore, the FTIR spectrum exhibits peaks typical for C_xN_y materials and is comparable with the spectra of previously reported C_1N_1 materials.^[9b,10b,15] Raman analysis displayed in **Figure 2b** shows features previously observed in C_1N_1 materials.^[9a] The small peak at 1001 cm^{-1} is typically assigned to the vibration of the triazine ring.^[16] The broad band from 1200 to 1800 cm^{-1} with local maxima at 1354 and 1514 cm^{-1} results from the overlap of triazine C–N and C–C vibrations.^[17] Peaks centered around 2600 cm^{-1}

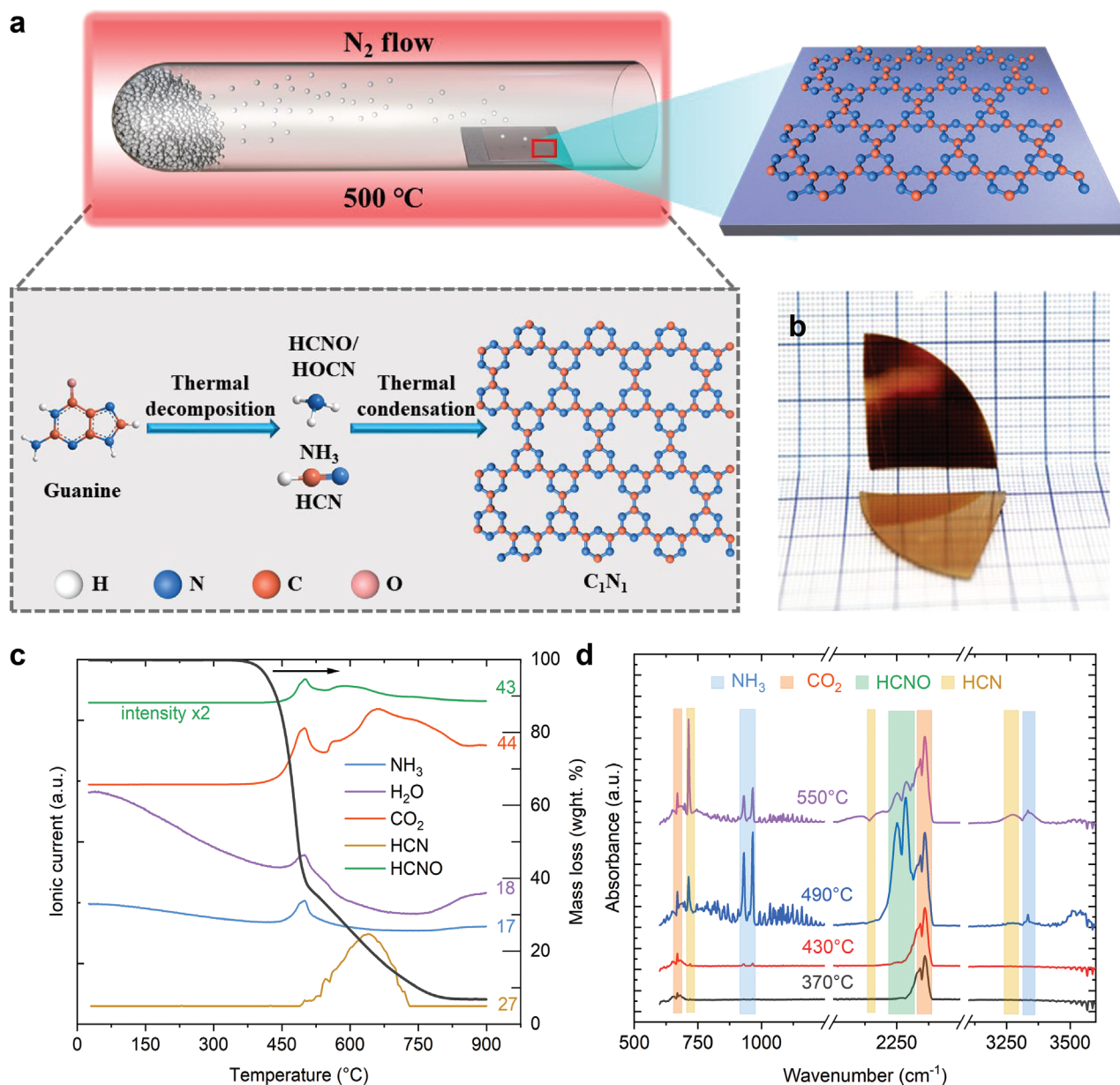


Figure 1. a) A schematic representation of the synthetic process, b) photo of prepared guanine based film on top of a fused silica substrate, c) TGA-MS of guanine, and d) FTIR of guanine decomposition products formed at different temperatures.

in Raman spectra are higher-order vibrations characteristic for stacking layers in carbonaceous materials.^[18] The peak at higher wavenumber, 2900 cm^{-1} , can be attributed to S3 peak, which is a second order peak originating in D-G combination.^[19] The optical properties of the film were determined by measuring its UV-vis absorption. The spectrum in Figure 2c shows a broad absorption without a well-defined peak. By constructing the Tauc plot, we determined the optical bandgap of the film to be 2.2 eV (inset Figure 2c). This value is smaller than theoretically predicted value of 2.89 to 2.72 eV.^[8]

The grazing angle incidence X-ray diffraction (XRD) pattern peak at 27.2° (Figure 2d) shows that the sample is formed by well-defined stacks of conjugated layers. The shoulder at 20° is

ascribed to the fused silica substrate. The calculated value of the interlayer distance is 3.28 Å. To better understand the structure of the synthesized C_1N_1 films, an idealized model of C_1N_1 was theoretically studied. The model was obtained by means of semi-local density functional theory (DFT) second-generation Car-Parrinello-based dynamical simulated annealing,^[20b] as implemented in the CP2K code.^[21] The energetically optimized and most stable structure of C_1N_1 consists of well-ordered carbon and nitrogen atoms that are alternately bonded to each other resulting in a porous graphitic-like structure with AA stacking (Figure 2e). The interlayer distance is 3.3 Å, which corresponds well to the above described 2θ value of 27.2° in the experimental XRD measurement (inset Figure 2d). To further

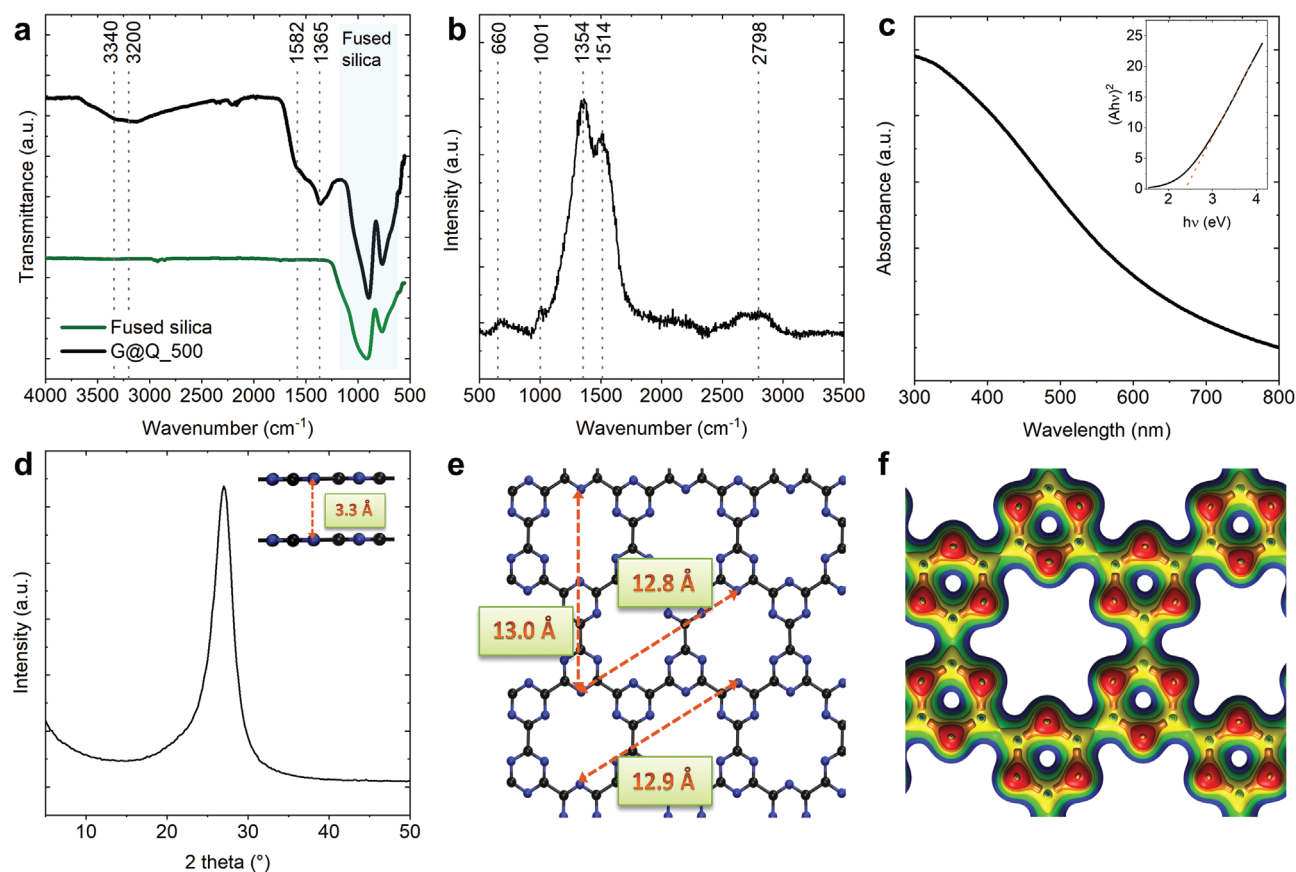


Figure 2. Physical characterization of guanine-derived film on fused silica substrate. a) FTIR spectrum of film on top of fused silica and of pure substrate. b) Raman spectrum. c) UV-visible absorption spectrum (inset, Tauc plot) of the film. d) Glancing incidence XRD using a glancing angle of 0.17° . The inset corresponds to the side view of the C_1N_1 model developed. e) Top view of the same model. The distances represented are the relevant distances for XRD measurements (carbon: black, nitrogen: blue). f) Top view of the electron density map of a C_1N_1 layer from low (model blue) to high electron density (red).

visualize the location of the electrons within the material, the electron density was calculated for the C_1N_1 layers and is illustrated as a 2D electron density heat map in Figure 2f. The electron density exhibits a patterned distribution, where the high electron density (red area) is accumulated at the more electronegative nitrogen atoms (DDEC6^[22] net atomic charge = -0.31). Accordingly, the carbon atoms are partially positively charged ($+0.31$) leading to C–N bond polarizations inside the material. In the idealized structural model in Figure 2e, we can observe long-range in plane periodicity with distances between 12.8 and 13.0 Å which corresponds to 2θ values of 6.8 – 6.9° . However, XRD data show only slightly elevated signal overlapping with the background preventing unambiguous assignment. This shows that the in-plane organization of the structure is distorted.

The distorted nature of the film was further confirmed by X-ray photoelectron spectroscopy (XPS) analysis. The analysis of the XPS spectra shows that the sample has a C/N ratio of 0.95, which is in agreement with EDX analysis. However, the deconvolution of the high-resolution C1s XPS spectra in Figure S1c in the Supporting Information shows the presence of three types of carbon atoms with peaks centered at 284.7 eV (C=C), at 285.9 eV (N=C(C)–N), and 287.2 eV (N–(N)C=N).^[23] From the theoretical structure, only one type of carbon can be

expected (i.e., N=C(C)–N). The peak at higher binding energy corresponds to carbon atoms typically found in carbon nitrides and bound to three nitrogen atoms. The presence of a peak corresponding to carbon not bound to nitrogen might be justified by the adventitious carbon which is almost always present on the surface of air exposed sample. Ladva et al. synthesized C_xN_y films (with C:H:N ratio of 1.2:1.4:1) by condensation of decomposition products of dicyanamide in LiBr:KBr salt mixture. They showed that the intense peak 284.6 eV quickly disappeared upon Ar cluster ion etching proving that the peak corresponded to environmental contamination.^[24] Further, the high-resolution N1s XPS spectra show the strongest peak centered at 398.1 eV and a much less intense peak at 399.7 eV. The first peak corresponds well to nitrogen from the triazine rings in C_1N_1 model structure. The second one can be assigned to C₃–N, typical for graphitic carbon nitrides. There is also a third weak peak at 401.0 eV which can be attributed to not condensed amino groups.^[23] This corroborates the FTIR analysis, where amino groups were clearly visible.

The obtained films have a composition very close to C_1N_1 , however, as can be seen from XRD and XPS analysis it contains many defects which are rather typical for carbon nitride family compounds, prepared by thermolysis reactions. For

instance in heptazine $g\text{-C}_3\text{N}_4$ the ratio between N1s XPS peaks from $\text{C}=\text{N}=\text{C}$ and $\text{N}-\text{C}_3$ should be 3, however, it is always significantly lower pointing at not complete condensation.^[23] Therefore, we expect the presence of a certain amount of condensed melamine-like motifs that provides distortion points to the structure. Such defects certainly occur from side reactions during condensation process of released nitrogen containing species. This explains why XRD shows a very intense stacking peak while the in-plane distances are almost absent. In this context, we would like to point out that model C_1N_1 structures have never been truly synthesized. All the previous reports fail to present the characterization data which could be unambiguously associated to a C_1N_1 theoretical phase.^[9b,10a,c] Probably, the closest structure to the theoretical model has been obtained by Feng and Li who referred to their material as C_3N_3 . They started from predefined triazine units of cyanuric chloride. By heating the precursor in the presence of a copper foil they forced the Ullmann reaction in which two aryl chlorides are coupled together. The resulting material had structural motifs similar to a model C_1N_1 phase, however, was stabilized by copper chloride embedded in the pores. Vertical orientation of $\text{Cu}-\text{Cl}$ bond in regard to CN plane induced higher separation between layers. Nevertheless, the removal of Cu caused immediate collapse of the structure. In alternative processes, the synthesis starts from smaller molecular species which built in situ the triazine units. The main difficulty arises most likely from formation of $\text{C}-\text{C}$ bonds between those units, as in most of the processes formation of $\text{N}-\text{C}_3$ bridges is much easier (as observed by numerous synthetic processes of $g\text{-C}_3\text{N}_4$).

To test the (photo)electrochemical properties of the films, the film needed to be deposited on a conductive substrate. The important advantage of the CVD process is its versatility in covering different surfaces and shapes. Therefore, the set of samples was prepared on top of FTO coated glass using the same protocol. However, three different amounts of guanine (1, 2, and 4 g) were tested and labeled FTO-O500-1, FTO-O500-2, and FTO-O500-4. Further, the films were characterized and compared with the sample on top of the fused silica substrate. SEM images (Figure S2, Supporting Information) revealed that the films on top of FTO coated glass are rougher and have shown a structure formed by colloid like particles. This can be caused by the rougher morphology of the substrate surface as well as by the catalytic activity of Sn in cyclotrimerization reaction since this reaction is catalyzed by a variety of transition metals.^[25] The composition of the films was measured with EDX and the C/N ratio was determined to be 1.1 for all the samples. The recorded FTIR and Raman spectra of the samples on top of FTO are in good agreement with the sample prepared on top of fused silica (Figure S3, Supporting Information). The thickness of the films was studied using atomic force microscopy. Results can be seen in Figure S4 and Table S1 in the Supporting Information. The determined thickness was 85.3, 55.8, and 65.8 nm for FTO-O500-1, FTO-O500-2, and FTO-O500-4, respectively. The thickness decreases with the amount of guanine used. This might seem at a first glance counterintuitive but it is easily explainable. Using larger amounts of guanine, the tube becomes faster saturated with precursors promoting gas-phase condensation which slows down the deposition on the substrate. This then results in depletion of reactants leading

to thinner film.^[26] The thickness measured by AFM is further in agreement with the electrochemical area measured by cyclic voltammetry. The highest one was obtained for FTO-O500-1 and similar for FTO-O500-2 and FTO-O500-4, see Figure S5 in the Supporting Information.

The photoresponse of guanine-based thin films was further studied at an applied bias of -0.5 V versus Ag/AgCl with periodic illumination of 10 s (see Figure 3a). The generated photocurrent is $11 \mu\text{A cm}^{-2}$ for FTO-O500-1, $6 \mu\text{A cm}^{-2}$ for FTO-O500-2, and sample FTO-O500-4 has a negligible photocurrent. Sample FTO-O500-1 shows immediate photocurrent with only negligible decay, meaning that the separation of generated electron-hole pairs is efficient and there is little to no recombination. On the other hand, sample FTO-O500-2 shows a curved profile in current increase after light on and in the decrease of current after light off. This means the generation of electron-hole pairs with light and the recombination after the light has been turned off is slower. The quick recombination of light-generated carriers in sample FTO-O500-4 leads to negligible photocurrent. Figure 3b shows the transient photovoltage of guanine-derived films under periodic illumination of 10 s. The value of open circuit potential changes by a value of 10 mV for FTO-O500-1, 20 mV for FTO-O500-2 and does not change in the case of FTO-O500-4. A smaller value of photovoltage in the case of FTO-O500-1 compared to FTO-O500-2 can be explained by the thickness of the film. Thicker film experiences more resistance loss, therefore the value of photovoltage is lower. In the case of FTO-O500-4, only tiny observable light response can be explained considering the synthesis conditions. We hypothesize that the use of larger amounts of precursor makes the tube very saturated with reactant intermediates in the gas phase.^[26] The intermediates have larger chances to interact which after deposition leads to a more defective structure. These defects can then serve as sites for the recombination of photogenerated carriers. Therefore there will be no or neglectable observable photoresponse. The direction of change upon illumination is toward the anodic potential region. That is because the quasi-Fermi level, or the electrochemical potential, of the electrons increases under illumination, meaning the material is a p-type semiconductor.^[27]

Figure 3c shows the cyclic voltammetry curve of FTO-O500-2 in dark and with light. The current density is the same in the forward bias and then higher with the light on in the reverse bias, this is because our material is a p-type semiconductor. The comparison of performance with literature shows that the films perform as good as other C_3N_4 films with similar thickness even when these are already doped with other heteroatoms (Table 1). The electrochemical behavior of FTO-O500-2 in the acidic electrolyte (Figure 3d) changes during cycling. At the beginning, we can observe capacitive behavior. During cycling the onset of hydrogen evolution reaction (HER) moves to lower potentials and after 50 cycles reaches only -350 mV against Ag/AgCl electrode, a value comparable to metal-based catalysts. This behavior was observed previously and is described as the so-called adjacent Tafel mechanism.^[28] This is proposed to occur in graphitic carbon materials, in which after activation with acids which consist on the intercalation of the acid ions, the onset of HER is very low. After such activation, our material exhibits higher HER current densities than previously reported

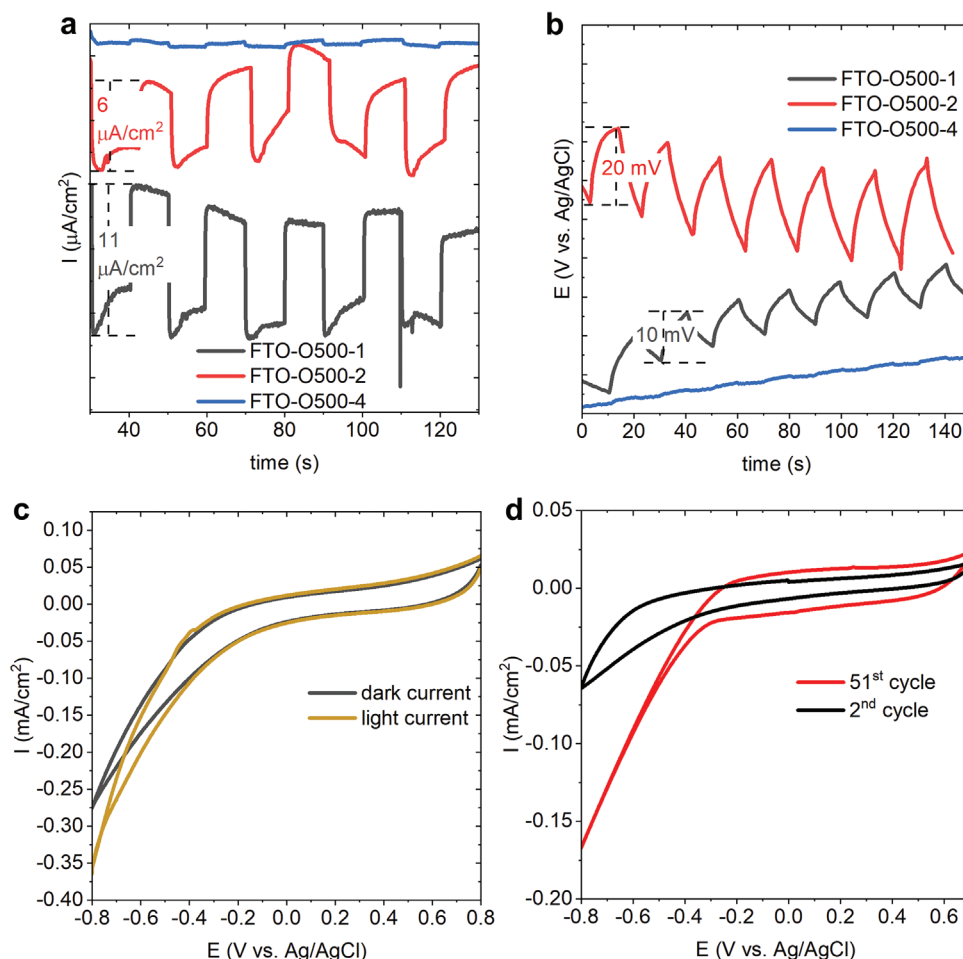


Figure 3. a) Transient photocurrent and b) photovoltage of guanidine-derived thin films on top of FTO at a bias of -0.5 V versus Ag/AgCl. c) Cyclic voltammometry of FTO-O500-2 with the light on and light off, 0.5 M H_2SO_4 used as an acidic electrolyte, Pt wire as a counter electrode (scan rate 20 mV s^{-1}). d) Evolution of cyclic voltammometry curves of FTO-O500-2 in the same conditions.

Table 1. Comparison of photocurrent and photovoltage of different carbon nitride based materials.

Material	Thickness	Applied bias	Photocurrent	Photovoltage	Reference
		V versus Ag/AgCl	$[\mu\text{A cm}^{-2}]$	[V]	
FTO-O500-1	85 nm	-0.5	11	0.10	This work
FTO-O500-2	55 nm	-0.5	6	0.20	This work
C_3N_5	–	-0.2 – 0.6	5–40	1.3	[30]
$\text{C}_3\text{N}_5/\text{NH}_2\text{-UiO-66}$	–	–	0.24	–	[31]
g- C_3N_4 -0.01	8 μm	–	60–130	–	[32]
$\text{MoS}_2/\text{S-doped g-C}_3\text{N}_4$ film	<100 nm	0.5	120	–	[33]
g- C_3N_4 film with thiourea	–	0.5	30	0.13	[34]
g- $\text{C}_3\text{N}_4/\text{rGO}$	36 μm	0.3	72	–	[35]
Crystal-face tailored C_3N_4	200 nm	1.23 vs RHE	228.2	–	[36]
SOCN film	55 nm	–	15	–	[37]
g- C_3N_4 on chalcopyrite film	200 μm	-0.5	5	1.50	[27]
Nanostructured C_3N_4	–	0.62	30.2	–	[38]
Porous carbon nitride film	8 μm	0.3	14	–	[39]

C₃N₄ film,^[27] even though our C₁N₁ film is thinner. Further, the onset potential is much lower than that reported for C₃N₃ and C₃N₃·CuCl, prepared from trichlorotriazine, which have onset of −0.747 and −0.547 V versus Ag/AgCl, respectively.^[29]

3. Conclusions

In this paper, we present a simple and versatile method for the preparation of C₁N₁ thin films. Using a simplified CVD process and guanine as a molecular precursor, we were able to obtain a homogeneous coating of surfaces. The thermal decomposition pathway of guanine was studied using TGA-MS and TGA-FTIR, the main decomposition products are ammonia, HCN, and HCNO/HNCO compounds. The composition was determined by EXD and for the film prepared on top of the fused silica substrate, the C/N ratio was 0.93, very close to the targeted ratio of 1. The films are p-type semiconductors with an optical bandgap of 2.2 eV. (Photo)electrochemical properties of the film are studied and the film shows a good photoresponse to visible light, exhibiting 20 mV photovoltage and 15 μA cm^{−2} photocurrent at a bias −0.5 V versus Ag/AgCl. Further, the C₁N₁ films are shown to be a prospective catalyst for HER, exhibiting adjacent Tafel mechanism in 0.5 M H₂SO₄. We believe that this results not only probe the validity of C₁N₁ films for (photo)electroapplications but also the synthetic approach here used can inspire other material scientist to use not toxic indirect precursors for the preparation of advanced thin film semiconductors.

4. Experimental Section

Materials: Guanine 99% was purchased from Merck and used as received. Fluorine doped tin oxide glass slides with surface resistivity ≈13 Ω sq^{−1} were purchased from Sigma-Aldrich. Fused silica substrates were purchased from Microchemicals. Glass substrates were purchased from Merck.

Synthesis: Substrates were first washed with distilled water, ethanol, and acetone and dried with compressed air. Guanine (1, 2, or 4 g) was placed at the end of a 110 mL glass test tube (19 cm length; 3 cm diameter) and cleaned substrates were placed at the other end. The test tube was put into a chamber oven with a nitrogen flow of 2 L min^{−1}. The chamber was flushed for 1 h with nitrogen prior to heating. The films were deposited for 1 h at 500 °C with a heating rate of 5 °C min^{−1}, the samples were then let to cool down naturally.

Characterization: Raman spectroscopy measurements were done using Confocal Raman Microscope Alpha 300 from WiTech equipped with neodymium-doped yttrium aluminum garnet laser with 532 nm wavelength. The morphology of the samples was investigated by SEM using a Zeiss Gemini 1550 microscope. Samples were coated with Au/Pd (80/20) before measurement, the approximate thickness of the metal layer is 5–10 nm. EDX spectroscopy was analyzed using an Oxford Instruments EDX analyzer coupled to the SEM. Elemental chemical analysis was carried out using a Vario MICRO cube carbon, hydrogen, nitrogen, oxygen and sulfur Elemental Analyzer (Elementar Analysensysteme GmbH, Langensfeld) in the carbon, hydrogen, nitrogen, and sulfur mode and a2mgChem80s Method. Approximately 20 samples prepared on top of glass were peeled off from the substrate using water, dried at 100 °C for 72 h and then analyzed. FTIR spectra were obtained using a Thermo Scientific Nicolet iD5 spectrometer. XPS measurements were performed on a ThermoScientific Escalab 250 Xi. A microfocused, monochromated Al Kα X-ray source (1486.68 eV) and a 400 μm spot size were used in the

analysis. Samples were prepared using carbon tape. LiCl was added to each sample to calibrate the binding energies toward Li. ThermoScientific Avantage software was used to analyze the resulting spectra. TGA was performed using a NETZSCHTG 209 F1 device in the range of 25–1000 °C in a nitrogen atmosphere, heating rate of 10 °C min^{−1} in a Pt crucible. TGA coupled with MS was performed using a thermos microbalance TG 209 F1 Libra with a Thermostat MS with ionization energy 75 eV. The measurement was done in a range of 25–910 °C, with a heating rate of 2.5 °C min^{−1} and a helium flow of 10 mL min^{−1}. The FTIR analysis of volatiles was recorded by FTIR spectrometer Tensor 27 (Bruker) equipped with a heated gas cell (250 °C) connected to NETZSCH STA 449F3 device via heated transfer line (250 °C). The measurement was performed in the heating range between 40 and 900 °C with a heating rate of 10 °C min^{−1} and nitrogen flow. The spectra were recorded with a spectral resolution of 4 cm^{−1} and 600 pts were registered per min.

Cyclic voltammetry measurements were done using a three-electrode electrochemical cell. Prepared films on FTO coated glass were employed as working electrodes with an area of 0.38 cm², platinum as a counter electrode, and an Ag/AgCl (sat. KCl) electrode as a reference. 0.5 M H₂SO₄ and 0.5 M phosphate buffer (pH 7) were used as electrolytes. The measurements were recorded on an MPG2 multichannel potentiostat from BioLogic. For the photoelectrochemistry measurements, the light emitting diode lamp with visible light was used. The lamp was placed beneath the electrochemical cell, which had a hole allowing the light to reach the working electrode.

Computational Details: Periodic density functional theory calculations were carried out using the hybrid Gaussian and plane wave approach,^[40] as implemented in the CP2K/Quickstep code.^[21] Therein, the Kohn–Sham orbitals are described by an accurate molecularly optimized double-zeta basis set with one additional set of polarization functions,^[41] while the charge density is represented by plane waves with a density cutoff of 500 Ry. The unknown exchange and correlation energy was approximated by the B97-D functional, which is based on Becke’s power-series Ansatz, plus a damped atom-pairwise dispersion correction to account for long-range van der Waals.^[42] Separable norm-conserving pseudopotentials were employed to mimic the interactions between the valence electrons and the ionic cores.^[43] The structure of C₁N₁ films was modeled using a supercell with $a = 14.8$, $b = 13.0$, and $c = 13.2$ Å and $\alpha = \beta = \gamma = 90.0^\circ$, which consists of four C₁N₁ layers. Optimized structures were obtained by globally minimizing the potential energy while varying the atomic positions by dynamical simulated annealing based on the second-generation Car-Parrinello approach of Kühne et al.^[20]

Supporting Information

Supporting Information is available from the Wiley Online Library or from the author.

Acknowledgements

The Max Planck Society is greatly acknowledged for financial support. M.O. acknowledges the Alexander Von Humboldt stiftung for financial support.

Conflict of Interest

The authors declare no conflict of interest.

Data Availability Statement

The data that support the findings of this study are available from the corresponding author upon reasonable request.

Keywords

C₁N₁, photoelectrochemistry, thin films

Received: September 16, 2022

Revised: October 31, 2022

Published online:

- [1] K. Sakaushi, M. Antonietti, *Acc. Chem. Res.* **2015**, *48*, 1591.
- [2] X. Wang, K. Maeda, A. Thomas, K. Takanabe, G. Xin, J. M. Carlsson, K. Domen, M. Antonietti, *Nat. Mater.* **2009**, *8*, 76.
- [3] a) J. Mahmood, E. K. Lee, M. Jung, D. Shin, I.-Y. Jeon, S.-M. Jung, H.-J. Choi, J.-M. Seo, S.-Y. Bae, S.-D. Sohn, N. Park, J. H. Oh, H.-J. Shin, J.-B. Baek, *Nat. Commun.* **2015**, *6*, 6486; b) Z. Tian, N. López-Salas, C. Liu, T. Liu, M. Antonietti, *Adv. Sci.* **2020**, *7*, 2001767.
- [4] L. Tan, C. Nie, Z. Ao, H. Sun, T. An, S. Wang, *J. Mater. Chem. A* **2021**, *9*, 17.
- [5] R. Zhang, B. Lia, J. Yang, *Nanoscale* **2015**, *7*, 14062.
- [6] A. Bafekry, C. Stampfl, S. F. Shayesteh, *ChemPhysChem* **2020**, *21*, 164.
- [7] J. Mahmood, E. K. Lee, M. Jung, D. Shin, H.-J. Choi, J.-M. Seo, S.-M. Jung, D. Kim, F. Li, M. S. Lah, N. Park, H.-J. Shin, J. H. Oh, J.-B. Baek, *Proc. Natl. Acad. Sci. U. S. A.* **2016**, *113*, 7414.
- [8] K. Srinivasu, B. Modak, S. K. Ghosh, *J. Phys. Chem. C* **2014**, *118*, 26479.
- [9] a) L. Liu, Y. Xia, J. Zhang, *RSC Adv.* **2014**, *4*, 59102; b) J. Zeng, Z. Chen, X. Zhao, W. Yu, S. Wu, J. Lu, K. P. Loh, J. Wu, *ACS Appl. Nano Mater.* **2019**, *2*, 7969.
- [10] a) Q. Guo, Q. Yang, C. Yi, L. Zhu, Y. Xie, *Carbon* **2005**, *43*, 1386; b) H. Yin, Q. Guo, D. He, J. Li, S. Sun, *RSC Adv.* **2017**, *7*, 44001; c) J. Feng, M. Li, *Adv. Funct. Mater.* **2020**, *30*, 2001502.
- [11] Y. A. Jeilani, P. N. Williams, S. Walton, M. T. Nguyen, *Phys. Chem. Chem. Phys.* **2016**, *18*, 20177.
- [12] P. Cheng, Y. Li, S. Li, M. Zhang, Z. Zhou, *Phys. Chem. Chem. Phys.* **2010**, *12*, 4667.
- [13] D. P. Glavin, M. Schubert, J. L. Bada, *Anal. Chem.* **2002**, *74*, 6408.
- [14] J. L. de la Fuente, M. Ruiz-Bermejo, D. Nna-Mvondo, R. D. Minard, *Polym. Degrad. Stab.* **2014**, *110*, 241.
- [15] J. Li, C. Cao, J. Hao, H. Qiu, Y. Xu, H. Zhu, *Diamond Relat. Mater.* **2006**, *15*, 1593.
- [16] a) P. J. Larkin, M. P. Makowski, N. B. Colthup, *Spectrochim. Acta, Part A* **1999**, *55*, 1011; b) P. Praus, L. Svoboda, M. Ritz, I. Troppová, M. Šihor, K. Kočí, *Mater. Chem. Phys.* **2017**, *193*, 438.
- [17] W. Sawodny, K. Niedenzu, J. W. Dawson, *J. Chem. Phys.* **1966**, *45*, 3155.
- [18] S. S. Nanda, M. J. Kim, K. S. Yeom, S. S. A. An, H. Ju, D. K. Yi, *Trends Anal. Chem.* **2016**, *80*, 125.
- [19] H. Wang, J. T. Robinson, X. Li, H. Dai, *J. Am. Chem. Soc.* **2009**, *131*, 9910.
- [20] a) T. D. Kühne, *WIREs Comput. Mol. Sci.* **2014**, *4*, 391; b) T. D. Kühne, M. Krack, F. R. Mohamed, M. Parrinello, *Phys. Rev. Lett.* **2007**, *98*, 066401; c) T. D. Kühne, E. Prodan, *Ann. Phys.* **2018**, *391*, 120.
- [21] T. D. Kühne, M. Iannuzzi, M. D. Ben, V. V. Rybkin, P. Seewald, F. Stein, T. Laino, R. Z. Khaliullin, O. Schütt, F. Schiffmann, D. Golze, J. Wilhelm, S. Chulkov, M. H. Bani-Hashemian, V. Weber, U. Borštnik, M. Taillefumier, A. S. Jakobovits, A. Lazzaro, H. Pabst, T. Müller, R. Schade, M. Guidon, S. Andermatt, N. Holmberg, G. K. Schenter, A. Hehn, A. Bussy, F. Belleflamme, G. Tabacchi, et al., *J. Chem. Phys.* **2020**, *152*, 194103.
- [22] T. A. Manz, N. G. Limas, *RSC Adv.* **2016**, *6*, 47771.
- [23] T. S. Miller, A. B. Jorge, T. M. Suter, A. Sella, F. Corà, P. F. McMillan, *Phys. Chem. Chem. Phys.* **2017**, *19*, 15613.
- [24] S. A. Ladva, W. Travis, R. Quesada-Cabrera, M. Rosillo-Lopez, A. Afandi, Y. Li, R. B. Jackman, J. C. Bear, I. P. Parkin, C. Blackman, C. G. Salzmann, R. G. Palgrave, *Nanoscale* **2017**, *9*, 16586.
- [25] T. Nagata, Y. Obora, *Asian J. Org. Chem.* **2020**, *9*, 1532.
- [26] Z. L. Wang, Y. Liu, Z. Zhang, in *Handbook of Nanophase and Nanostructured Materials*, Springer, Boston, MA **2003**.
- [27] F. Yang, M. Lublow, S. Orthmann, C. Merschjann, T. Tyborski, M. Rusu, S. Kubala, A. Thomas, R. Arrigo, M. Hävecker, T. Schedel-Niedrig, *ChemSusChem* **2012**, *5*, 1227.
- [28] R. K. Das, Y. Wang, S. V. Vasilyeva, E. Donoghue, I. Pucher, G. Kamenov, H.-P. Cheng, A. G. Rinzler, *ACS Nano* **2014**, *8*, 8447.
- [29] J. Feng, M. Li, *Adv. Funct. Mater.* **2020**, *30*, 2001502.
- [30] P. Kumar, E. Vahidzadeh, U. K. Thakur, P. Kar, K. M. Alam, A. Goswami, N. Mahdi, K. Cui, G. M. Bernard, V. K. Michaelis, K. Shankar, *J. Am. Chem. Soc.* **2019**, *141*, 5415.
- [31] B. Wu, T. Sun, N. Liu, L. Lu, R. Zhang, W. Shi, P. Cheng, *ACS Appl. Mater. Interfaces* **2022**, *14*, 26742.
- [32] H. Yu, R. Shi, Y. Zhao, T. Bian, Y. Zhao, C. Zhou, G. I. N. Waterhouse, L.-Z. Wu, C.-H. Tung, T. Zhang, *Adv. Mater.* **2017**, *29*, 1605148.
- [33] L. Ye, D. Wang, S. Chen, *ACS Appl. Mater. Interfaces* **2016**, *8*, 5280.
- [34] L. Ye, S. Chen, *Appl. Surf. Sci.* **2016**, *389*, 1076.
- [35] Z. Chen, A. Huang, K. Yu, T. Cui, Z. Zhuang, S. Liu, J. Li, R. Tu, K. Sun, X. Tan, J. Zhang, D. Liu, Y. Zhang, P. Jiang, Y. Pan, C. Chen, Q. Peng, Y. Li, *Energy Environ. Sci.* **2021**, *14*, 3430.
- [36] W. Xiong, S. Chen, M. Huang, Z. Wang, Z. Lu, R.-Q. Zhang, *ChemSusChem* **2018**, *11*, 2497.
- [37] M. Huang, H. Wang, W. Li, Y.-L. Zhao, R.-Q. Zhang, *J. Mater. Chem. A* **2020**, *8*, 24005.
- [38] J. Liu, H. Wang, Z. P. Chen, H. Moehwald, S. Fiechter, R. van de Krol, L. Wen, L. Jiang, M. Antonietti, *Adv. Mater.* **2015**, *27*, 712.
- [39] G. Peng, L. Xing, J. Barrio, M. Volokh, M. Shalom, *Angew. Chem., Int. Ed.* **2018**, *57*, 1186.
- [40] G. Lippert, J. Hutter, M. Parrinello, *Mol. Phys.* **1997**, *92*, 477.
- [41] J. VandeVondele, J. Hutter, *J. Chem. Phys.* **2007**, *127*, 114105.
- [42] E. Perlt, P. Ray, A. Hansen, F. Malberg, S. Grimme, B. Kirchner, *J. Chem. Phys.* **2018**, *148*, 193835.
- [43] S. Goedecker, M. Teter, J. Hutter, *Phys. Rev. B* **1996**, *54*, 1703.